

1 **Upper tropospheric water vapour variability at high latitudes**
2 **– Part 1: Influence of the annular modes**

3 **C. E. Sioris^{1*}, J. Zou², D. A. Plummer³, C. D. Boone⁴, C. T. McElroy¹, P. E. Sheese²,**
4 **O. Moeini¹, P. F. Bernath^{4,5}**

5 [1] {Department of Earth and Space Science and Engineering, York University, Toronto,
6 Canada, 4700 Keele St., Toronto, ON, Canada, M3J 1P3}

7 [2] {Department of Physics, University of Toronto, 60 St. George. St., Toronto, ON, Canada,
8 M5S 1A7}

9 [3] {Canadian Centre for Climate Modelling and Analysis, Environment Canada, Victoria, BC,
10 Canada}

11 [4] {Department of Chemistry, University of Waterloo, 200 University Ave. W, Waterloo, ON,
12 Canada, N2L 3G1}

13 [5] {Department of Chemistry & Biochemistry, Old Dominion University, 4541 Hampton Blvd.,
14 Norfolk, VA, USA, 23529}

15 Correspondence to:

16 C. E. Sioris (csioris@sdcnlab.esse.yorku.ca)

17

18

19

20

21

22

23

24

25

26

27

28

29

30

31

32

33

34

35

36

1 **Abstract**

2 Seasonal and monthly zonal medians of water vapour in the upper troposphere and lower
3 stratosphere (UTLS) are calculated for both Atmospheric Chemistry Experiment (ACE)
4 instruments for the northern and southern high-latitude regions (60-90°N and 60-90°S). Chosen
5 for the purpose of observing high-latitude processes, the ACE orbit provides sampling of both
6 regions in eight of 12 months of the year, with coverage in all seasons. The ACE water vapour
7 sensors, namely MAESTRO (Measurements of Aerosol Extinction in the Stratosphere and
8 Troposphere Retrieved by Occultation) and the Fourier Transform Spectrometer (ACE-FTS) are
9 currently the only satellite instruments that can probe from the lower stratosphere down to the
10 mid-troposphere to study the vertical profile of the response of UTLS water vapour to the
11 annular modes.

12 The Arctic oscillation (AO), also known as the northern annular mode (NAM), explains 64%
13 ($r=-0.80$) of the monthly variability in water vapour at northern high-latitudes observed by ACE-
14 MAESTRO between 5 and 7 km using only winter months (January to March, 2004-2013).
15 Using a seasonal timestep and all seasons, 45% of the variability is explained by the AO at
16 6.5 ± 0.5 km, similar to the 46% value obtained for southern high latitudes at 7.5 ± 0.5 km
17 explained by the Antarctic oscillation or southern annular mode (SAM). A large negative AO
18 event in March 2013 produced the largest relative water vapour anomaly at 5.5 km (+70%) over
19 the ACE record. A similarly large event in the 2010 boreal winter, which was the largest
20 negative AO event in the record (1950-2015), led to >50% increases in water vapour observed by
21 MAESTRO and ACE-FTS at 7.5 km.

22

23

24

25

26

1 1 Introduction

2 Water vapour is the most important greenhouse gas in the atmosphere (Lacis et al., 2010) playing
3 an important role in climate change by magnifying changes in radiative forcing by longer-lived
4 greenhouse gases through the water vapour feedback (Dessler and Sherwood, 2009). A variety of
5 observations have shown that, at near-global scales, specific humidity in the troposphere has
6 been increasing along with atmospheric temperatures in a manner consistent with that predicted
7 by the Clausius-Clapeyron equation – approximately 7%/K (Hartmann et al., 2013). Long-term
8 increases in water vapour are expected in the troposphere due to long-term increases in
9 temperature and the resulting exponential increase in saturation vapour pressure (Soden and
10 Held, 2006). In the middle stratosphere, long-term changes in water vapour may result from
11 changes in the temperature of the tropical tropopause ‘coldpoint’ that controls the dehydration of
12 tropospheric air as it enters the stratosphere (Brewer, 1949) and from changes in its stratospheric
13 source gas, namely methane (Oman et al., 2008). Water vapour in the extratropical lowermost
14 stratosphere may be additionally influenced by changes in isentropic transport from the
15 subtropics (Dessler et al., 2013). Additionally, absorption by atmospheric water vapour of
16 radiation at terahertz and radio frequencies is a serious impediment for radio astronomy and for
17 long-distance communications (Suen et al., 2014). The vertical distribution of water vapour is
18 relevant for all of the effects mentioned.

19 In order to understand and attribute long term changes, internal modes of variability, particularly
20 those with longer periods, should be considered simultaneously. In the extratropics, the annular
21 modes explain more of the month-to-month and year-to-year variance of the atmospheric flow
22 than any other climatic phenomenon (Thompson and Wallace, 2000;
23 <http://www.atmos.colostate.edu/ao/introduction.html>). The northern and southern annular modes
24 (NAM, SAM), also known as the Arctic oscillation (AO) and Antarctic oscillation (AAO)
25 respectively, produce a strong zonal flow at mid-latitudes during their positive phase with an
26 equatorward meridional flow near 60° latitude and weaker zonal flow accompanied by an
27 increased tendency for poleward flow during the negative phase (Thompson and Wallace, 2000).
28 In the high-latitude upper troposphere, where water vapour enhancements due to evaporation at
29 the surface are minor relative to the lower troposphere, it is the negative phase of the annular
30 modes that is expected to increase water vapour by increased transport from more humid lower

1 latitudes. Devasthale et al. (2012) used the Atmospheric Infrared Sounder (AIRS) on the Aqua
2 satellite to study the longitudinal and vertical structure of water vapour in the 67-82°N band and
3 interpreted the observed structure by separating the observations according to the phases of the
4 Arctic oscillation. To our knowledge, no one has studied the impact of the Antarctic oscillation
5 on upper tropospheric water vapour (UTWV).

6 The AO exhibits the largest variability during the cold season (Thompson and Wallace, 2000).
7 Groves and Francis (2002) related TOVS (TIROS Operational Vertical Sounder) precipitable
8 water vapour net fluxes across 70°N in winter to the phase of the AO. Li et al. (2014) showed
9 that the longwave radiative forcing anomaly due to NAM-related variability of cold season water
10 vapour for the 2006 to 2011 period at northern high latitudes is small ($\sim -0.2 \text{ W/m}^2$).

11 Here, the relationship between water vapour in the upper troposphere and lower stratosphere
12 (UTLS) at northern and southern high-latitudes (60-90°N and 60-90°S) and their respective
13 annular modes is studied using observations from satellite-based limb profilers. A particular
14 focus is the height dependence of the relationship: does it extend up to or above the tropopause?

15 **2 Method**

16 **2.1 Satellite observations**

17 SCISAT was launched in 2003 carrying a suite of solar occultation instruments to carry out the
18 mission named the Atmospheric Chemistry Experiment (ACE) (Bernath et al., 2005). The ACE
19 instruments measuring water vapour are Measurements of Aerosol Extinction in the Stratosphere
20 and Troposphere Retrieved by Occultation (MAESTRO, McElroy et al., 2007) and the Fourier
21 Transform Spectrometer (FTS, Bernath et al., 2005). The ACE datasets begin in February 2004.
22 The measurements provide a unique combination of high vertical resolution and the ability to
23 measure the water vapour profile from the mid-troposphere to the lower stratosphere where the
24 volume mixing ratio (VMR) is < 10 ppm (parts per million), below the lower detection limit of
25 the nadir-sounding AIRS (Gettelman et al., 2004). HIRS (High-Resolution Infrared Radiation
26 Sounder) is the nadir sounder used in the last two Intergovernmental Panel on Climate Change
27 (IPCC) assessments (e.g. Hartmann et al., 2013) for long-term trend studies of upper
28 tropospheric humidity (Soden et al., 2005; Shi and Bates, 2011). However, the trend analysis of
29 the HIRS dataset is confined to the region 60°N to 60°S (Bates and Jackson, 2001). The

1 Tropospheric Emission Spectrometer (TES) should also be mentioned, but in polar regions at
2 pressures < 400 mb, the vertical resolution of TES is 11.6 km (Worden et al., 2004). IASI
3 (Infrared Atmospheric Sounding Interferometer) water vapour retrievals have coarse poor
4 vertical resolution in the polar upper troposphere and the upper altitude limit of the retrieval only
5 approaches the tropopause (Herbin et al., 2009; Wiegeler et al., 2014). Other current limb
6 sounders include the sub-millimetre radiometer on Odin which can only measure in the upper
7 troposphere in the tropics (Rydberg et al., 2009) and the Microwave Limb Sounder on Aura
8 which can only probe down to 316 mb (~8 km) (Su et al., 2006). The fact that MAESTRO and
9 ACE-FTS are on the same platform is extremely valuable for comparing the month-to-month
10 variations of atmospheric constituents observed by both instruments.

11 The MAESTRO water vapour retrieval method follows the one used previously (Sioris et al.,
12 2010). Data are available at https://database.scisat.ca/level2/mae_water/ after user registration.
13 Some of the main algorithm changes are described here. The maximum allowable optical depth
14 in the water vapour fitting window (926.0-969.7 nm) is reduced from 7.63 to 6.7. This reduces
15 the number of noisy spectra but also possibly increases susceptibility to a dry bias at the lowest
16 altitudes. Also, MODTRAN 5.2 (Berk, 2013) is now used for forward modelling. The water
17 vapour absorption line intensities are mostly from Brown et al. (2002) and have uncertainties of
18 2-5%, an improvement relative to the previous version (Sioris et al., 2010) which used
19 MODTRAN 4 (relying on HITRAN 1996). Water vapour profiles are retrieved from all available
20 MAESTRO optical depth spectra (version 3.12, spanning 2004 to 2013) from the ongoing ACE
21 mission. For version 3.12 optical depth spectra, the tangent height registration relies on matching
22 simulated O₂ slant columns obtained from air density profiles, based on temperature and pressure
23 retrieved from ACE-FTS (Boone et al., 2013), with slant columns observed by MAESTRO using
24 the O₂ A band. MAESTRO water vapour mixing ratios that are more than twice as large as all
25 other mixing ratios at any altitude in the same month were examined in detail and filtered if
26 related to a measurement problem. Significant outliers are not numerous and no recursion is
27 necessary. No other filtering is necessary. ACE-FTS gridded version 3.5 data are used in the
28 study. The FTS retrieval is described by Boone et al. (2013). ACE-FTS water vapour with
29 retrieval uncertainty of >100% are filtered as well as data points that are significantly negative
30 (i.e. magnitude of mixing ratio is greater than retrieval uncertainty). Polar Ozone and Aerosol

1 Measurement III (POAM III) water vapour measurements are also used to compare the observed
2 seasonal cycle. Only version 4 data (Lumpe et al., 2006) with a flag of 0 are used.

3 **2.2 Retrieval uncertainties and validation**

4 POAM III has been validated down to 8 km or ~300 mb (Nedoluha et al., 2002; Lumpe et al.,
5 2006) and this is used as the POAM III lower altitude limit in this work. Previous comparisons
6 between MAESTRO and ACE-FTS have been favourable (Sioris et al., 2010, Carleer et al.,
7 2008). ACE-FTS water vapour has been used in the validation of other instruments (e.g. Lambert
8 et al., 2007) and in the Stratospheric Processes And their Role in Climate (SPARC) Data
9 Initiative (Hegglin et al., 2013). Waymark et al. (2013) compared version 3 ACE-FTS water
10 vapour data with the previous well-validated version 2.2 (e.g. Carleer et al., 2008) and found 2%
11 differences over a large altitude range. Since the MAESTRO tangent height registration has
12 improved substantially since the previous publication (Sioris et al., 2010), the current version of
13 MAESTRO water vapour profiles has been validated in a global sense versus ACE-FTS in the
14 companion paper (Sioris et al., 2015).

15 Beside the validation results, it is also valuable to look at retrieval uncertainties to understand the
16 expected data quality. Based on an analysis of one year of southern high-latitude data, the
17 MAESTRO water vapour retrieval relative uncertainty is found to be best at the lowest retrieval
18 altitude of 5 km and is typically ~30% for a 0.4 km thick layer. The smallest retrieval relative
19 uncertainty of 2% for ACE-FTS occurs typically at 8.5 km (considering 5.5 to 19.5 km) and
20 rapidly deteriorates below 7 km to 15% based on northern high-latitude data (2004-2013) on a 1
21 km altitude grid.

22 **2.3 Tropopause definitions**

23 For the northern hemisphere, the monthly tropopause height is defined by the lower of the
24 thermal tropopause or the lowest height at which the lapse rate is <2 K/km in monthly median
25 temperatures from the Global Environmental Multiscale (GEM) regional assimilation system
26 (Laroche et al., 1999). In the southern hemisphere, due to the extreme cold in the winter lower
27 stratosphere, the tropopause is defined as the lower of the thermal tropopause or the lowest
28 height at which the lapse rate is 2 K/km in monthly maximum temperatures from the GEM
29 assimilation system. The lapse rate tropopause concept has been used previously for the

1 extratropics (e.g. Randel et al., 2012). With this definition, the climatological tropopause at
2 southern high latitudes is at 10.5 km for the winter half of the year (May-October) and at 9.5 km
3 in the summer half (November to April).

4 **2.4 Anomalies**

5 To arrive at water vapour anomalies, there are three steps: creation of the time series (e.g.
6 monthly or seasonal), compilation of the climatology, and deseasonalization. To create monthly
7 medians for northern high latitudes, occultation profiles in the 60-90°N latitude band are
8 selected. At southern high latitudes (60-90°S), monthly means are preferred particularly for
9 MAESTRO instead of medians to avoid a low bias in the widely dehydrated winter lower
10 stratosphere. The sampling provided by the ACE orbit as a function of latitude and month is
11 illustrated by Randel et al. (2012). The consequence of the non-uniform latitudinal sampling as a
12 function of month for the purpose of this study is discussed in Sect. 2.5. This sampling pattern
13 repeats annually. Because ACE instruments sample southern high latitudes in only eight of
14 twelve calendar months, November, January, March-May and July-September represent spring,
15 summer, autumn and winter, respectively, when a seasonal timescale is used. In the north,
16 climatological values are obtained for all calendar months except April, June, August, and
17 December. The seasonal anomalies use the following groupings: winter consists of January and
18 February, spring includes March and May, summer is composed of July and September and the
19 fall is represented by October and November.

20 Vertically, the binning is done in 1.0 km intervals centered between 5.5 km and 22.5 km (above
21 23 km, the MAESTRO water vapour absorption signal tends to be below the lower detection
22 limit). The monthly mean at a given altitude bin is included in the climatology and anomaly
23 dataset if there are ≥ 20 observations per month. A single MAESTRO profile can supply more
24 than one observation per altitude bin since the water vapour retrieval is done on the tangent
25 height (TH) grid, which is as fine as 0.4 km at the lowest TH of 5 km and as the angle widens
26 between line-of-sight and the orbital track. The same process is followed with ACE-FTS and
27 POAM III data to generate monthly median and mean time series.

28 The monthly climatology, used to deseasonalize the time series, is generated by averaging the
29 monthly medians and means over the available years. Figure 1 illustrates the bias between
30 MAESTRO and ACE-FTS water vapour climatologies at both high latitude bands. An ACE-FTS

1 high bias of ~10% has been observed for the extratropical upper troposphere (40-80°N and 40-
2 80°S, near 300 hPa) (Hegglin et al., 2013). While inconclusive, a general wet bias between 5 and
3 8 km is also suggested by lidar comparisons in the extratropics (Carleer et al., 2008; Moss et al.,
4 2013). Accounting for an upper tropospheric +10% wet bias in ACE-FTS, MAESTRO and ACE-
5 FTS agree within $\pm 20\%$ at all heights (5.5-17.5 km, in 1 km steps) in both hemispheres at high
6 latitudes.

7 At each height, the monthly climatology (e.g., Fig. 4) is subtracted from the time series (e.g., Fig.
8 3) to give the absolute deseasonalized anomaly. Dividing the monthly absolute anomaly by the
9 monthly climatology gives the relative anomaly. Note that July and August 2011 were omitted
10 from the MAESTRO southern high latitude climatology at 6.5-9.5 km due to a ~50%
11 enhancement at these altitudes due to the Puyehue volcanic eruption (Sioris et al., 2015). The
12 same process is followed to generate anomalies of temperature, relative humidity (RH),
13 tropopause pressure, and tropopause height. The anomalies of relative humidity with respect to
14 ice are based on pressure and temperature from the GEM assimilation system and an accurate
15 saturation vapour pressure formulation (Murray, 1967). The latitude sampling anomaly is
16 generated by calculating the average sampled latitude for each high-latitude band and then the
17 mission-averaged latitude in each high-latitude band is subtracted.

18 Note that, because conclusions below about the importance of the annular modes are reached
19 based on water vapour anomalies and the fact the deseasonalization is sensor-specific (i.e. the
20 time series observed by each instrument is deseasonalized using its own climatology), overall
21 biases and seasonally-dependent biases are actually inconsequential. Relevant biases are
22 discussed in Sect. 2.5.

23 **2.5 Regression analysis**

24 We use a multiple linear regression analysis to determine the contribution of the appropriate
25 annular mode to the variability in deseasonalized water vapour at high latitudes as a function of
26 altitude. The set of available basis functions include a linear trend, the monthly AAO (Mo,
27 2000) and AO (Larson et al., 2005) indices (<http://www.cpc.noaa.gov/products/precip/CWlink/>)
28 and a latitude sampling anomaly time series. This basis function is included to illustrate that
29 sampling biases are minor even on a monthly time scale (using only the eight months which

1 sample each high-latitude region). Note that the AO index is calculated following the method of
2 Thompson and Wallace (2000).

3 When determining the response of water vapour to the AO, the AO index plus a constant are
4 used, and the linear trend is included if it is significant at the 1 standard error (σ) level. When
5 examining trend uncertainty reduction (Sect. 4.1), the regression uses a linear trend, plus a
6 constant; the annular mode index term is included for trend determination if it improves the trend
7 uncertainty without biasing the trend at the 1σ level.

8 The types of biases that could affect the analysis of water vapour variability are due to:

- 9 1) latitudinal sampling non-uniformity (Toohey et al., 2013),
- 10 2) interannual biases.

11 Regarding the non-uniform sampling of latitudes by the ACE orbit mentioned in Sect. 2.4, the
12 correlation between monthly time series of average sampled latitude in the northern high-latitude
13 region and the Arctic oscillation index is 0.19 and similarly the correlation between the monthly
14 time series of average sampled latitude in the southern high-latitude region and the Antarctic
15 oscillation index is 0.12. Given these very low correlations, ACE's latitudinal sampling should
16 have a negligible impact on any conclusion about the response of the observed water vapour
17 anomaly to the annular modes, although this is tested below using the latitude sampling anomaly
18 as a basis function. Toohey et al. (2013) estimated monthly mean sampling biases in the UTLS to
19 be $\leq 10\%$ for the category of instruments that includes ACE-FTS (and MAESTRO). The
20 interannual biases are also $< 10\%$ given that Sect. 3.2 below shows that approximately half of the
21 southern high-latitude water vapour seasonal anomaly (typically $\pm 10\%$ in amplitude) can be
22 explained by interannual variability in the Antarctic oscillation (i.e. real dynamical variability,
23 not artificial instrument-related variability). Also, there are no known issues with either
24 MAESTRO or ACE-FTS specific to a certain year. Furthermore, the self-calibrating nature of
25 solar occultation, combined with the wavelength stability of spectrometers (relative to filter
26 photometers) minimize interannual bias for MAESTRO and ACE-FTS. For example, any
27 variation in the optical (or quantum) efficiency of the instrument does not need to be calibrated
28 as it does with an instrument measuring nadir radiance.

1 **3 Results**

2 The MAESTRO water vapour record (Fig. 2) at southern high latitudes is similar to the records
3 of contemporary limb sounders as shown in Fig. 13 of Hegglin et al. (2013). The southern high-
4 latitude time series has slightly less water in the UTLS in late winter than at northern high-
5 latitudes (Fig. 3) due to the colder air temperatures.

6 **3.1 Seasonal cycle**

7 The dehydration in September that extends downward into the upper troposphere at southern
8 high-latitudes (Fig. 4) is clearly observed by MAESTRO annually (Fig. 2).

9 The variability in the UTWV at southern high latitudes on a monthly timescale is dominated by
10 the seasonal cycle. The observed seasonal variation is a factor of ~ 5 at 8.5 km (Fig. 5). The
11 seasonal cycle in water vapour is consistent with the ratio of maximum to minimum saturation
12 vapour mixing ratio at 8.5 km of 4.6 (± 1 standard deviation: 3.9-5.3), obtained for a typical year,
13 namely 2010, using analysis temperatures and pressures from the GEM assimilation system,
14 sampled at ACE measurement locations for January and August, the months corresponding to the
15 maximum and minimum water vapour in ACE-FTS and POAM III data at 8.5 km, respectively.
16 The approximate equality between the seasonal cycle amplitudes of observed and saturation
17 VMR in the troposphere implies a much weaker seasonal cycle in RH. The strong seasonal cycle
18 in UTWV is in stark contrast to weak (30%) seasonal variations in lower stratospheric (13.5 km)
19 monthly means, according to MAESTRO observations. The large seasonal cycle amplitude in
20 saturation vapour mixing ratio in the lower stratosphere is largely due to the extremely cold
21 temperatures in September.

22 The stronger seasonal cycle at northern high-latitudes (e.g. at 5.5 km, Fig. 6) is partly due to the
23 non-uniform latitudinal sampling differences in the months of maximum and minimum water
24 vapour VMR, particularly in the southern hemisphere. The northern hemisphere seasonal cycle
25 amplitude vertical profile (Fig. 6) is thus a truer reflection of the amplitude of the seasonal cycle
26 at $\sim 70^\circ\text{N}$. Figures 5 and 6 illustrate that the seasonal cycle amplitude of observed water vapour
27 VMR in the lower stratosphere departs from the seasonal cycle amplitude of the saturated VMR
28 due to the isolation of this overlying atmospheric region from large sources of water vapour.
29 According to GEM temperature analyses, the amplitude of the seasonal cycle in temperature is

1 18 K with a sharp peak in mid-summer (e.g. July) and generally sufficient to explain the seasonal
2 variation and its vertical dependence in the upper troposphere (Fig. 6).

3 In spite of the large tropospheric seasonality at high latitudes, it is possible to deseasonalize the
4 water vapour records from the ACE instruments and investigate the remaining sources of
5 temporal variability, as shown next.

6 **3.2 Antarctic oscillation**

7 At 8.5 km, where the largest anti-correlations exist between MAESTRO water vapour at 8.5 km
8 and the AAO index, it is observed that the relative standard error on the AAO fitting coefficient
9 is reduced when the regression is performed using a seasonal timestep rather than a monthly
10 timestep. Thus, in Fig. 7, the MAESTRO and ACE-FTS seasonal median relative anomaly for
11 8.5 ± 0.5 km and 7.5 ± 0.5 km, respectively, are presented. The use of medians is preferable for
12 detecting the AAO response in the troposphere where the water vapour mixing ratios are not
13 normally distributed. The monthly medians are also less susceptible to outliers in the individual
14 retrieved profiles. The large positive anomaly in 2011 is due to the most explosive eruption of a
15 volcano in the last 24 years, namely Puyehue, and will be discussed in the companion paper
16 (Sioris et al., 2015).

17 At 8.5 km, where the response of water vapour to AAO has the smallest relative
18 uncertainty for both ACE-FTS and MAESTRO, the response ranges between +23% and -18%
19 for individual seasons and the standard deviation of the AAO response time series is 10% (2004-
20 2012). The anomalies in the upper troposphere are highly correlated with each other (e.g. $R =$
21 0.79 for MAESTRO absolute anomalies at 8.5 versus 9.5 km on a monthly timescale). In the
22 stratosphere (altitude ≥ 10 km), the response of MAESTRO water vapour to AAO is weak (not
23 significant). Figure 8 illustrates the vertical profile of the AAO response. There is a strong
24 vertical correlation between the water vapour responses to the AAO observed by the two
25 instruments and the responses are statistically significant (up to the 4σ level for ACE-FTS at 7.5
26 km) in the 5.5-8.5 km for both instruments indicating that the AAO affects water vapour
27 throughout the upper troposphere at southern high latitudes. The MAESTRO and ACE-FTS
28 AAO fitting coefficients are not different from 0 at the 1σ level at 10.5 and 11.5 km,
29 respectively. Slight differences between the ACE instruments may relate to differences in their

1 respective fields of view (FOV). MAESTRO's FOV is 1 km in the vertical direction, whereas
2 ACE-FTS, because of its 3.7 km circular field of view at a tangent point 10 km above the
3 ground, will see some contribution from the troposphere even when the FOV is centered 1.5 km
4 above the tropopause. Given that the ACE-FTS field of view is circular, the full-width at half-
5 maximum of the FOV is 3.2 km. Due to vertical oversampling of the FOV, the vertical resolution
6 of the water vapour products from each ACE instrument is finer than the height of the FOV (see
7 also Sioris et al, 2010). Nevertheless, differences in vertical resolution between the ACE
8 instruments will lead to a slight difference in terms of the peak altitude of the anti-correlation
9 between the water vapour anomaly and AAO. The impact of non-uniform latitudinal sampling is
10 deferred to Sect. 3.3. The response profile of saturation volume mixing ratio to the AAO is also
11 shown and is discussed in Sect. 4.2.

12 As stated in Sect. 1, the AO is most active in the winter when the surface is coldest.
13 Therefore less infrared (IR) radiation is emitted and trapped by AO-related increases in
14 atmospheric water vapour. Over Antarctica, the AAO instead shows strength in late spring
15 (Thompson and Wallace, 2000) at a time when there is increased IR radiation emitted by the
16 surface, possibly making AAO-related water vapour changes more likely to lead to increases in
17 temperature at the surface and to reduce outgoing longwave flux at the top of the atmosphere
18 (TOA). The impact of AAO-induced variability of upper tropospheric water vapour on surface
19 climate and outgoing longwave flux at the top of the atmosphere is assessed for November 2009
20 and November 2010, two months when the AAO was of opposite phase (see Appendix A for
21 details of the method). The cooling rate differences at the surface between these negative and
22 positive phases of the AAO are trivial ($< 0.07\text{K}$) in late spring (November). The outgoing
23 longwave flux is reduced by 0.7 W/m^2 in November 2009 relative to November 2010 due solely
24 to AAO-related upper tropospheric changes in water vapour. Scaling this change to the typical
25 AAO fluctuation in all seasons (1979-2014), variations of 0.2 W/m^2 in the outgoing longwave
26 flux at the TOA are found, which are equal to the magnitude Li et al. (2014) found for the AO-
27 related IR flux changes at TOA due to water vapour for the Arctic cold season. Note that Li et al.
28 (2014) found the AO-related water vapour changes to be much smaller than AO-related cloud
29 changes.

1 3.3 Arctic oscillation

2 Figure 9 shows the altitude dependence of observed water vapour response to the Arctic
3 oscillation using all eight months that sample the northern high-latitude region. There is a
4 coherent and statistically significant response (up to the 4σ level for MAESTRO) to the AO
5 observed by both instruments, with a general decrease through the upper troposphere and a
6 vanishing response in the vicinity of the tropopause. Above 12 km, the response to the AO is
7 insignificant at the 1σ level. The magnitude of the response to the AO is also similar to the
8 magnitude of the response of UTWV at southern high latitudes to the Antarctic oscillation.

9 The spatiotemporal sampling of ACE (Bernath et al., 2005) is quite non-uniform on monthly
10 time scales whereas on seasonal timescales the spatial coverage of the entire high-latitude region
11 becomes more complete. When the latitudinal sampling anomaly is used as a basis function, it is
12 generally not a significant term in either hemisphere. Fig. 9 shows that the inclusion of this term
13 does not change the response to the AO, reinforcing the same finding for the response to the
14 AAO (Fig. 8). Clearly, water vapour at high-latitudes is responding with high fidelity to the local
15 annular mode.

16 Using the MAESTRO water vapour anomalies, a seasonal timestep and all seasons, 45% of the
17 variability is explained at 6.5 ± 0.5 km, similar to the fraction obtained for southern high latitudes.

18 The most active season for the AO is from January to March based on standard deviations of the
19 AO index in the period from 1950 to 2015. This three month period was used by Thompson and
20 Wallace (2000). Figure 10 shows a water vapour anomaly time series for an altitude of 6.5 km,
21 composed only of January, February and March (2004-2013). The wintertime anti-correlation
22 between the ACE-FTS water vapour anomaly and the AO index peaks at 6.5 km with $R = -0.57$.
23 MAESTRO shows a much stronger anti-correlation of $R = -0.80$ at 6.5 and 5.5 km. A large
24 negative AO event in March 2013 produced the largest relative water vapour anomaly at 5.5 km
25 (+70%) over the MAESTRO record. March 2013 was not available below 8 km for ACE-FTS
26 but at 8.5 and 9.5 km, ACE-FTS and MAESTRO both show the largest positive anomalies for
27 any March in either northern high-latitude data record (+32 and +35% at 8.5 km and +16 and
28 +27% at 9.5 km for MAESTRO and ACE-FTS, respectively) and a vanishing enhancement at
29 10.5 km (above the monthly mean tropopause). A similarly large event in winter 2010, which
30 was the largest negative AO event in the record (1950-2015), led to >50% and 30% increases in

1 northern high-latitude water vapour observed at 7.5 km in January and February 2010,
2 respectively, with agreement between MAESTRO and ACE-FTS. January 2010 has the largest
3 anomaly at 7.5 km in any month (considering all seasons) of the northern high-latitude data
4 records of MAESTRO and ACE-FTS. Steinbrecht et al. (2011) used a multiple linear regression
5 analysis to demonstrate a significant increase in total column ozone (+8 Dobson units) in the
6 winter of 2010 that was attributed to the same historically strong negative phase of the Arctic
7 oscillation.

8 **4 Discussion and conclusions**

9 Polar regions have a strong seasonal cycle in UTWV, driven by the seasonality of the local
10 temperature. In the Arctic upper troposphere, condensation and precipitation play a minor role in
11 governing the water vapour abundance on monthly timescales. Near the Arctic tropopause (250-
12 350 mb), cloud fractions are <35% (Treffeisen et al., 2007) and MAESTRO monthly median
13 relative humidity at 9.5 km is < 40% in all 63 months in which this instrument has observed the
14 northern high-latitude region. However, dynamical variability via the annular modes has been
15 shown here to strongly affect UTWV at high latitudes. Apart from the seasonal cycle, the
16 Antarctic oscillation is a dominant mode of variability in upper tropospheric (~8 km) water
17 vapour at southern high latitudes on a seasonal timescale and the Arctic oscillation explains most
18 of the variability at wintertime UTWV in northern high latitudes.

19 **4.1 Impact of fitting annular mode indices on decadal trends**

20 In the most recent IPCC report, Hartmann et al. (2013) review the literature on trends in UTWV
21 observed from satellite instruments. Only one such publication is cited, namely Shi and Bates
22 (2011). This work uses HIRS data between 85°N and 85°S, but only trends at low latitudes
23 (30°N-30°S) are discussed. While long-term trends in polar UTWV require continued
24 measurements and investigation, including the AO index in the trend analysis improves trend
25 uncertainties below 12 km over the MAESTRO record (e.g. by 16% at 6.5 km) and reduces a
26 statistically insignificant (1σ) but consistent, positive bias in the decadal trend (2004-2013) that
27 is found when the AO is excluded from the regression model. This bias stems from the two large
28 negative events in the winters of 2010 and 2013 which lie near the end of the data record. The
29 trend uncertainty reduction is 22% upon inclusion of the Antarctic Oscillation Index into

1 regression modelling of the linear trend in water vapour at 8.5 km at southern high-latitudes,
2 again with no significant impact on the linear trend itself.

3 **4.2 Proposed mechanisms**

4 The amplitude of the response by water vapour to annular mode oscillations does not change
5 significantly (1σ) whether UTWV is binned versus altitude or geopotential altitude in either
6 hemisphere at high latitudes, indicating the insensitivity to the choice of vertical coordinate. This
7 is important to note that as the correlation of other atmospheric variables with the annular modes
8 is explored in this section.

9 There is some observational evidence for two mechanisms that could explain how UTWV at
10 high latitudes responds to the annular modes. The first is through annular-mode-related air
11 temperature fluctuations, which impact UTWV by changing the saturation mixing ratio. For
12 changes in saturation mixing ratio to have an impact, there needs to be an available supply of
13 upper tropospheric water vapour. The second mechanism is through changes to the meridional
14 flux itself (e.g. Devasthale et al., 2012; Thompson and Wallace, 2000), given the latitudinal
15 gradient in water vapour between high and mid-latitudes at all upper tropospheric heights.

16 The response profile of saturation VMR relative anomalies (from analyses of the GEM
17 assimilation system) to the AAO (Fig. 8) is studied in order to gain insight into the relative
18 contribution of the two proposed mechanisms. The ability to distinguish between the two
19 mechanisms using saturation VMR anomalies requires that the mechanisms are not correlated
20 spatially with each other to a high degree. This has been verified using the latitude and altitude
21 dependence of their responses to the annular modes (Thompson and Wallace, 2000). The two
22 mechanisms are complementary in that they both increase UTWV at high latitudes during the
23 negative phase of the local annular mode.

24 Below 9 km, this response tends to be weaker than the response by deseasonalized water vapour
25 observed by the ACE instruments, implying that the temperature mechanism cannot fully explain
26 the strong observed response of water vapour at southern high latitudes. Near the tropopause
27 (9.5-10.5 km), the response of saturation VMR to the AAO becomes effectively zero (within
28 1σ), but the response of observed water vapour to the AAO is also decreasing considerably
29 relative to lower altitudes. The response of water vapour to the AAO differs significantly

1 between MAESTRO and ACE-FTS except at 5.5 and 6.5 km, making it generally difficult to
2 unequivocally determine the relative contribution of the two proposed mechanisms.
3 Nevertheless, there is an obvious need for a mechanism in addition to the temperature-related
4 one to explain the observed response of water vapour in the southern high latitudes upper
5 troposphere. The effectiveness of the meridional flux mechanism during negative AAO periods
6 is amplified by the large latitudinal gradients in water vapour between this isolated region and
7 southern mid-latitudes.

8 At northern high latitudes, saturation VMR responds to the AO in a similar fashion to its
9 response to the AAO at southern high latitudes (Figs. 8-9). The response of saturation VMR to
10 the AO at northern high latitudes tends to be smaller in magnitude than the response by water
11 vapour inferred from ACE observations, but the difference is not statistically significant at all
12 altitudes compared to the ACE-FTS water vapour response. The water vapour anomalies from
13 the two ACE instruments show a decreasing response to the AO with increasing altitude at
14 northern high latitudes, but generally differ in the magnitude of the response, as is the case as
15 well at southern high-latitudes. Thus, no general conclusion can be unequivocally drawn about
16 the relative contribution of the two proposed mechanisms in the northern high latitude upper
17 troposphere.

18 We see no evidence in either high-latitude region of a third mechanism whereby the UTWV
19 anomalies are simply explained by annular-mode-driven tropopause variations: the correlation
20 between tropopause height or tropopause pressure anomalies and the relevant annular mode is
21 not significant in either high-latitude region ($-0.1 < R < 0.1$). This is not surprising given that the
22 magnitude of responses of water vapour and saturation VMR to the annular modes diminish with
23 increasing height toward the tropopause.

24 Longer datasets and further analysis would be helpful to understand the contribution by each
25 proposed mechanism.

26

27 **Appendix A: Cooling rate differences**

1 Cooling rate vertical profiles are calculated using MODTRAN5.2 (e.g. Bernstein et al., 1996)
2 assuming an Antarctic surface altitude of 2.5 km, subarctic summer temperature profile, free
3 tropospheric aerosol extinction (visibility of 50 km) and two water vapour cases:
4 (1) using MAESTRO climatological median water vapour between 6.5 and 9.5 km increased by
5 the vertically-resolved water vapour response to AAO determined by multiple linear regression
6 (with AAO and constant as the only predictors) for November 2009, when the AAO was in its
7 negative phase (index of -1.92).
8 (2) same as (1), except for November 2010, when AAO index was +1.52 (positive phase).

9 **Acknowledgements**

10 The availability of the NOAA annular modes indices is appreciated. The ACE mission is
11 supported primarily by the Canadian Space Agency. POAM III data were obtained from the
12 NASA Langley Research Center Atmospheric Science Data Center. CES acknowledges Kaley
13 Walker (University of Toronto) for her role in including MAESTRO in the Water Vapour
14 Assessment (WAVAS) 2, organized by SPARC (Stratosphere-Troposphere Processes and their
15 Role in Climate). CES is grateful to Frédéric Laliberté (Environment Canada) for a helpful
16 discussion on separating the contributions by the two mechanisms proposed in Sect. 4.2.

17 **References**

18 Bates, J. J. and Jackson, D. L.: Trends in upper-tropospheric humidity, *Geophys. Res. Lett.*, 28,
19 1695-1698, 2001.
20 Berk, A.: Voigt equivalent widths and spectral-bin single-line transmittances: Exact expansions
21 and the MODTRAN®5 implementation, *J. Quant. Spectrosc. Radiat. Transfer*, 118, 102-120,
22 2013.
23 Bernath, P. F., McElroy, C. T., Abrams, M. C., Boone, C. D., Butler, M., Camy-Peyret, C.,
24 Carleer, M., Clerbaux, C., Coheur, P.-F., Colin, R., DeCola, P., DeMazière, M., Drummond, J.
25 R., Dufour, D., Evans, W. F. J., Fast, H., Fussen, D., Gilbert, K., Jennings, D. E., Llewellyn, E.
26 J., Lowe, R. P., Mahieu, E., McConnell, J. C., McHugh, M., McLeod, S. D., Michaud, R.,
27 Midwinter, C., Nassar, R., Nichitiu, F., Nowlan, C., Rinsland, C. P., Rochon, Y. J., Rowlands,
28 N., Semeniuk, K., Simon, P., Skelton, R., Sloan, J. J., Soucy, M.-A., Strong, K., Tremblay, P.,
29 Turnbull, D., Walker, K. A., Walkty, I., Wardle, D. A., Wehrle, V., Zander, R., and Zou, J.:

1 Atmospheric Chemistry Experiment (ACE): mission overview, *Geophys. Res. Lett.*, 32, L15S01,
2 doi:10.1029/2005GL022386, 2005.

3 Bernstein, L. S., Berk, A., Acharya, P. K., Robertson, D. C., Anderson, G. P., Chetwynd, J. H.,
4 and Kimball, L. M.: Very narrow band model calculations of atmospheric fluxes and cooling
5 rates, *J. Atmos. Sci.*, 53, 2887-2904, 1996.

6 Brown, L. R., Toth, R. A., and Dulick, M.: Empirical line parameters of H₂¹⁶O near 0.94 μm:
7 Positions, intensities and air-broadening coefficients, *J. Mol. Spectrosc.*, 212, 57-82, 2002.

8 Boone, C. D., Walker, K. A., Bernath, P. F., Version 3 retrievals for the Atmospheric Chemistry
9 Experiment Fourier Transform Spectrometer (ACE-FTS). The Atmospheric Chemistry
10 Experiment ACE at 10: A Solar Occultation Anthology, P. F. Bernath (Editor), A. Deepak
11 Publishing, Hampton, Virginia, 2013.

12 Brewer, A. W.: Evidence for a world circulation provided by the measurements of helium and
13 water vapour distribution in the stratosphere, *Q. J. Royal Met. Soc.*, 75, 351-363, 1949.

14 Carleer, M., Boone, C. D., Walker, K. A., Bernath, P. F., Strong, K., Sica, R. J., Randall, C. E.,
15 Vömel, H., Kar, J., Höpfner, M., Milz, M., von Clarmann, T., Kivi, R., Valverde-Canossa, J.,
16 Sioris, C. E., Izawa, M. R. M., Dupuy, E., McElroy, C. T., Drummond, J. R., Nowlan, C. R.,
17 Zou, J., Nichitiu, F., Lossow, S., Urban, J., Murtagh, D., and Dufour, D. G.: Validation of water
18 vapour profiles from the Atmospheric Chemistry Experiment (ACE), *Atmos. Chem. Phys.*
19 *Discuss.*, 8, 4499-4559, 2008.

20 Dessler, A. E. and Sherwood, S. C.: A matter of humidity, *Science*, 323, 1020-1021, doi:
21 10.1126/science.1171264, 2009.

22 Dessler, A. E., Schoeberl, M. R., Wang, T., Davis, S. M., and Rosenlof, K. H.: Stratospheric
23 water vapor feedback, *Proc. Natl. Acad. Sci.*, 110, 8087–18091, 2013.

24 Devasthale, A., Tjernström, M., Caian, M., Thomas, M. A., Kahn, B. H., and Fetzer, E. J.:
25 Influence of the Arctic Oscillation on the vertical distribution of clouds as observed by the A-
26 Train constellation of satellites, *Atmos. Chem. Phys.*, 12, 10535–10544, 2012.

27 Gettelman, A., Weinstock, E. M., Fetzer, E. J., Irion, F. W., Eldering, A., Richard, E. C.,
28 Rosenlof, K. H., Thompson, T. L., Pittman, J. V., Webster, C. R., and Herman, R. L.: Validation

1 of Aqua satellite data in the upper troposphere and lower stratosphere with in situ aircraft
2 instruments, *Geophys. Res. Lett.*, 31, L22107, doi:10.1029/2004GL020730, 2004.

3 Groves, D. G., Francis, J. A.: Variability of the Arctic atmospheric moisture budget from TOVS
4 satellite data, *J. Geophys. Res.* 107(D24), 4785, doi:10.1029/2002JD002285, 2002.

5 Hartmann, D. L., Klein Tank, A. M. G., Rusticucci, M., Alexander, L.V., Brönnimann, S.,
6 Charabi, Y., Dentener, F. J., Dlugokencky, E. J., Easterling, D. R., Kaplan, A., Soden, B. J.,
7 Thorne, P. W., Wild M., and Zhai, P.M.: Observations: Atmosphere and Surface. In: *Climate*
8 *Change 2013: The Physical Science Basis. Contribution of Working Group I to the Fifth*
9 *Assessment Report of the Intergovernmental Panel on Climate Change* [Stocker, T.F., D. Qin,
10 G.-K. Plattner, M. Tignor, S.K. Allen, J. Boschung, A. Nauels, Y. Xia, V. Bex and P.M. Midgley
11 (eds.)]. Cambridge University Press, Cambridge, United Kingdom and New York, NY, USA,
12 2013.

13 Hegglin, M. I., Tegtmeier, S., Anderson, J., Froidevaux, L., Fuller, R., Funke, B., Jones, A.,
14 Lingenfelter, G., Lumpe, J., Pendlebury, D., Remsberg, E., Rozanov, A., Toohey, M., Urban, J.,
15 von Clarmann, T., Walker, K. A., Wang, R., and K. Weigel: SPARC Data Initiative: Comparison
16 of water vapor climatologies from international satellite limb sounders, *J. Geophys. Res. Atmos.*,
17 118, 11824-11846, doi:10.1002/jgrd.50752, 2013.

18 Herbin, H., Hurtmans, D., Clerbaux, C., Clarisse, L., and Coheur, P.-F.: H₂¹⁶O and HDO
19 measurements with IASI/MetOp, *Atmos. Chem. Phys.*, 9, 9433–9447, 2009.

20 Lacis, A. A., Schmidt, G. A., Rind, D., Ruedy, R. A.: Atmospheric CO₂: Principal control knob
21 governing Earth's temperature, *Science*, 330, 356-359, 2010.

22 Lambert, A., Read, W. G., Livesey, N. J., Santee, M. L., Manney, G. L., Froidevaux, L., Wu, D.
23 L., Schwartz, M. J., Pumphrey, H. C., Jimenez, C., Nedoluha, G. E., Cofield, R. E., Cuddy, D.
24 T., Daffer, W. H., Drouin, B. J., Fuller, R. A., Jarnot, R. F., Knosp, B. W., Pickett, H. M., Perun,
25 V. S., Snyder, W. V., Stek, P. C., Thurstans, R. P., Wagner, P. A., Waters, J. W., Jucks, K. W.,
26 Toon, G. C., Stachnik, R. A., Bernath, P. F., Boone, C. D., Walker, K. A., Urban, J., Murtagh,
27 D., Elkins, J. W., and Atlas, E.: Validation of the Aura Microwave Limb Sounder middle
28 atmosphere water vapor and nitrous oxide measurements, *J. Geophys. Res.*, 112, D24S36, doi:
29 10.1029/2007JD008724, 2007.

1 Laroche, S., Gauthier, P., St-James, J., Morneau, J.: Implementation of a 3D variational data
2 assimilation system at the Canadian Meteorological Centre. Part II: The regional analysis,
3 *Atmos. Ocean*, 37, 281–307, 1999.

4 Larson, J., Zhou, Y., Higgins, R. W.: Characteristics of landfalling tropical cyclones in the
5 United States and Mexico: Climatology and interannual variability, *J. Clim.*, 18, 1247-1262,
6 2005.

7 Li, Y., Thompson, D. W. J., Huang, Y., Zhang, M.: Observed linkages between the northern
8 annular mode/North Atlantic Oscillation, cloud incidence, and cloud radiative forcing, *Geophys.*
9 *Res. Lett.*, 41, 1681–1688, doi:10.1002/2013GL059113, 2014.

10 Lumpe, J., Bevilacqua, R., Randall, C., Nedoluha, G., Hoppel, K., Russell, J., Harvey, V. L.,
11 Schiller, C., Sen, B., Taha, G., Toon, G., and Vömel, H.: Validation of Polar Ozone and Aerosol
12 Measurement (POAM) III version 4 stratospheric water vapor, *J. Geophys. Res.*, 111, D11301,
13 doi:10.1029/2005JD006763, 2006.

14 McElroy, C. T., Nowlan, C. R., Drummond, J. R., Bernath, P. F., Barton, D. V., Dufour, D. G.,
15 Midwinter, C., Hall, R. B., Ogyu, A., Ullberg, A., Wardle, D. I., Kar, J., Zou, J., Nichitiu, F.,
16 Boone, C. D., Walker, K. A., and Rowlands, N.: The ACE-MAESTRO instrument on SCISAT:
17 description, performance, and preliminary results, *Appl. Opt.*, 46, 4341–4356, 2007.

18 Mo, K. C.: Relationships between low-frequency variability in the southern hemisphere and sea
19 surface temperature anomalies. *J. Clim.*, 13, 3599-3610, 2000.

20 Moss, A., Sica, R. J., McCullough, E., Strawbridge, K., Walker, K., and Drummond, J.:
21 Calibration and validation of water vapour lidar measurements from Eureka, Nunavut, using
22 radiosondes and the Atmospheric Chemistry Experiment Fourier Transform Spectrometer,
23 *Atmos. Meas. Tech.*, 6, 741–749, 2013.

24 Murray, F. W.: On the computation of saturation vapor pressure, *J. Appl. Meteorol.*, 6, 203-204,
25 1967.

26 Nedoluha, G. E., Bevilacqua, R. M., Hoppel, K. W., Lumpe, J. D., and Smit, H.: Polar Ozone
27 and Aerosol Measurement III measurements of water vapor in the upper troposphere and
28 lowermost stratosphere, *J. Geophys. Res.*, 107, ACH 7-1 – ACH 7-10, 10.1029/2001JD000793,
29 2002.

1 Oman, L., Waugh, D. W., Pawson, S., Stolarski, R. S., and Nielsen, J. E.: Understanding the
2 changes of stratospheric water vapor in coupled chemistry–climate model simulations, *J. Atmos.*
3 *Sci.*, 65, 3278-3291, 2008.

4 Randel W. J., Moyer E., Park M., Jensen E., Bernath P., Walker K., and Boone C.: Global
5 variations of HDO and HDO/H₂O ratios in the upper troposphere and lower stratosphere derived
6 from ACE-FTS satellite measurements, *J. Geophys. Res.*, 117, D06303,
7 doi:10.1029/2011JD016632, 2012.

8 Shi, L., and Bates, J. J.: Three decades of intersatellite-calibrated High–Resolution Infrared
9 Radiation Sounder upper tropospheric water vapor, *J. Geophys. Res.*, 116, D04108,
10 doi:10.1029/2010JD014847, 2011.

11 Sioris, C. E., Zou, J., McElroy, C. T., McLinden, C. A., Vömel, H.: High vertical resolution water
12 vapour profiles in the upper troposphere and lower stratosphere retrieved from MAESTRO solar
13 occultation spectra, *Adv. Space Res.*, 46, 642–650, 2010.

14 Sioris, C. E., Zou, J., McElroy, C. T., Boone, C. D., Sheese, P. E., and Bernath, P. F.: Water
15 vapour variability in the high-latitude upper troposphere – Part 2: Impact of volcanic emissions,
16 *Atmos. Chem. Phys. Discuss.*, 15, 25873–25905, 2015.

17 Soden, B.J., Jackson, D. L., Ramaswamy, V., Schwarzkopf, M. D., Huang, X.:
18 The radiative signature of upper tropospheric moistening, *Science*, 310, 841-844, 2005.

19 Soden, B. J. and Held, I. M.: An assessment of climate feedbacks in coupled ocean-atmosphere
20 models, *J. Clim.*, 19, 3354-3360, doi:10.1175/JCLI3799.1, 2006.

21 Steinbrecht, W., Köhler, U., Claude, H., Weber, M., Burrows, J. P., and van der A, R. J.: Very
22 high ozone columns at northern mid-latitudes in 2010, *Geophys. Res. Lett.* 38: L06803,
23 doi:10.1029/2010GL046634, 2011.

24 Su, H., Read, W. G., Jiang, J. H., Waters, J. W., Wu, D. L., and Fetzer, E. J.: Enhanced positive
25 water vapor feedback associated with tropical deep convection: New evidence from Aura MLS,
26 *Geophys. Res. Lett.*, 33, L05709, doi:10.1029/2005GL025505, 2006.

1 Suen, J. Y., Fang, M. T., and Lubin, P. M.: Global distribution of water vapor and cloud cover
2 sites for high-performance THz applications, *IEEE Trans. Terahertz Sci. Technol.*, 4, 86-100,
3 2014.

4 Thompson, D. W. J., Wallace, J. M.: Annular modes in the extratropical circulation. Part I:
5 Month-to-month variability, *J. Clim.*, 13, 1000-1016, 2000.

6 Toohey, M., Hegglin, M. I., Tegtmeier, S., Anderson, J., Añel, J. A., Bourassa, A., Brohede, S.,
7 Degenstein, D., Froidevaux, L., Fuller, R., Funke, B., Gille, J., Jones, A., Kasai, Y., Krüger, K.,
8 Kyrölä, E., Neu, J. L., Rozanov, A., Smith, L., Urban, J., von Clarmann, T., Walker, K. A., and
9 R. H. J. Wang: Characterizing sampling biases in the trace gas climatologies of the SPARC Data
10 Initiative, *J. Geophys. Res. Atmos.*, 118, 11847–11862, doi:10.1002/jgrd.50874, 2013.

11 Treiffesen, R., Krejci, R., Ström, J., Engvall, A. C., Herber, A., and Thomason, L., Humidity
12 observations in the Arctic troposphere over Ny-Ålesund, Svalbard based on 15 years of
13 radiosonde data, *Atmos. Chem. Phys.*, 7, 2721–2732, 2007.

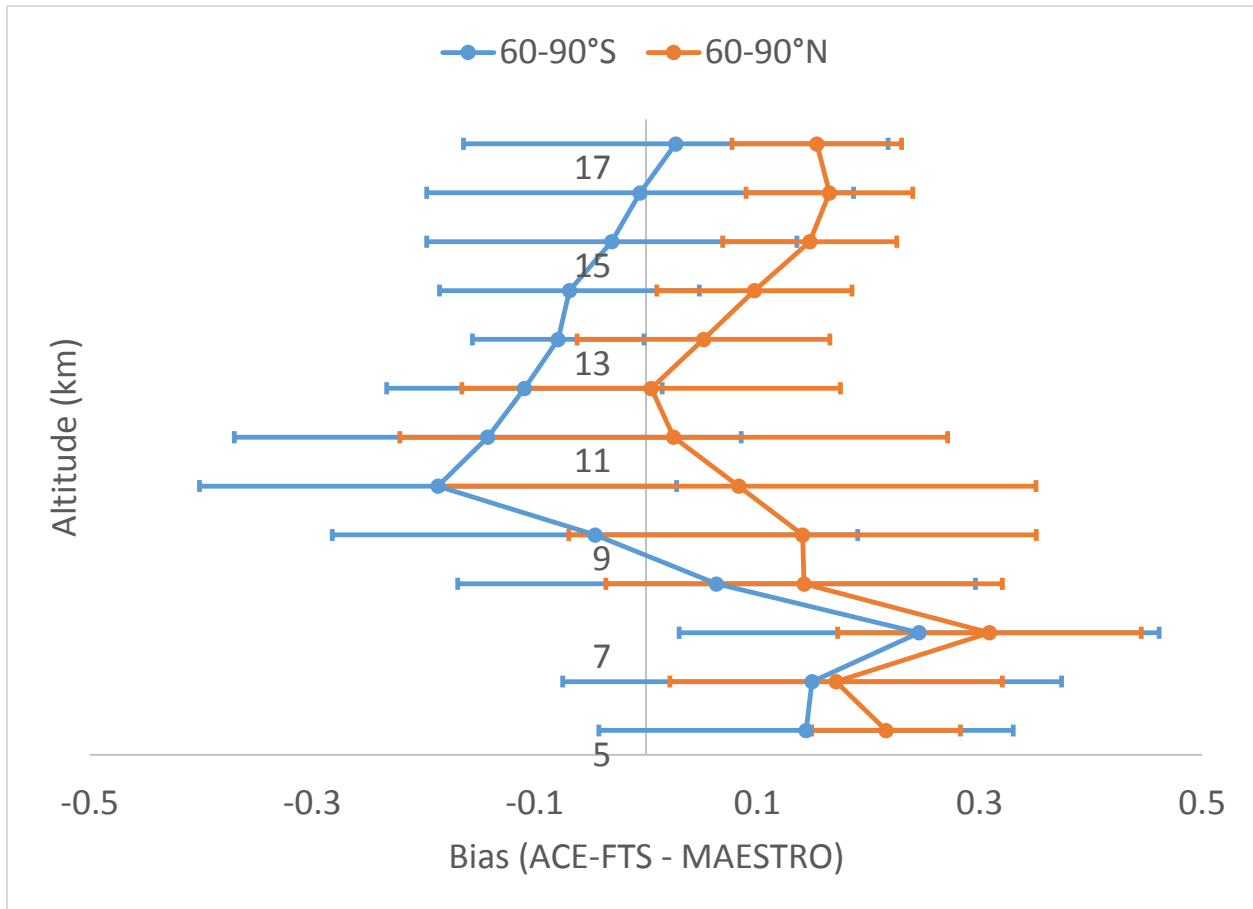
14 Waymark, C., Walker, K. A., Boone, C. D., and Bernath, P. F.: ACE-FTS version 3.0 data set:
15 validation and data processing update, *Annals of Geophys.*, 56, doi:10.4401/ag-6339, 2013.

16 Wiegele, A., Schneider, M., Hase, F., Barthlott, S., García, O. E., Sepúlveda, E., González, Y.,
17 Blumenstock, T., Raffalski, U., Gisi, M., and Kohlhepp, R.: The MUSICA MetOp/IASI H₂O and
18 δD products: characterisation and long-term comparison to NDACC/FTIR data, *Atmos. Meas.*
19 *Tech.*, 7, 2719–2732, 2014.

20 Worden, J., Kulawik, S. S., Shephard, M. W., Clough, S. A., Worden, H., Bowman, K., and
21 Goldman, A.: Predicted errors of tropospheric emission spectrometer nadir retrievals from
22 spectral window selection, *J. Geophys. Res.*, 109, D09308, doi:10.1029/2004JD004522, 2004.

23
24
25
26
27
28

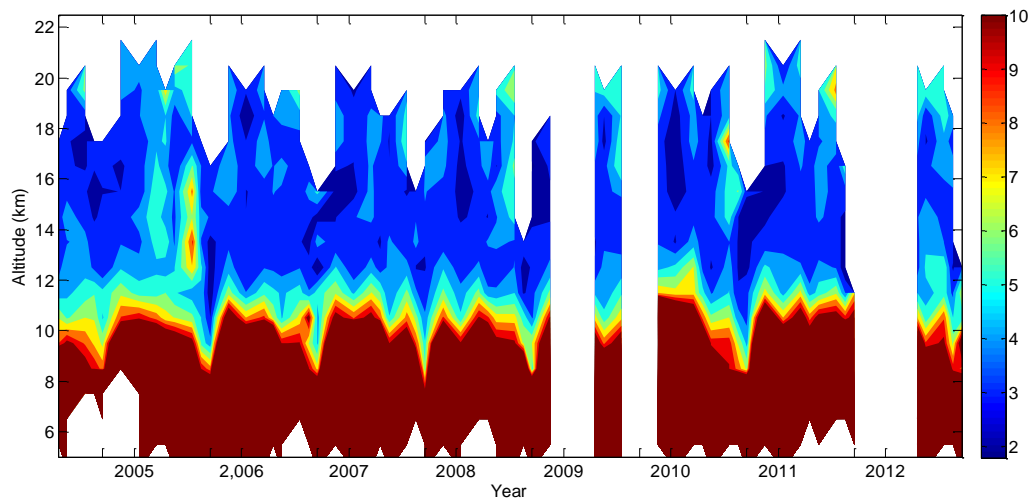
1



2

3 Figure 1. (orange) Relative differences between ACE-FTS and MAESTRO climatological
4 medians averaged over the eight months sampling the northern high-latitude region and their
5 standard deviation; (blue) relative differences between ACE-FTS and MAESTRO climatological
6 means averaged over the eight months sampling the southern high-latitude region and their
7 standard deviation. The horizontal bars show the standard deviation of the differences between
8 the two climatologies over the eight available months. To account for vertical resolution
9 differences, the MAESTRO climatology was vertically smoothed with a 3 km boxcar.

10



1

2 Figure 2. Time series of the MAESTRO monthly mean water vapour volume mixing ratio
 3 (VMR) versus altitude (5.5-22.5 km) at southern high latitudes (60-90°S) with a linear colour
 4 scale (ppm), emphasizing the stratospheric variability. Unlabelled ticks along the bottom
 5 correspond to September. The time series is composed using the eight months in which ACE
 6 samples the southern high latitudes (see Sect. 2).

7

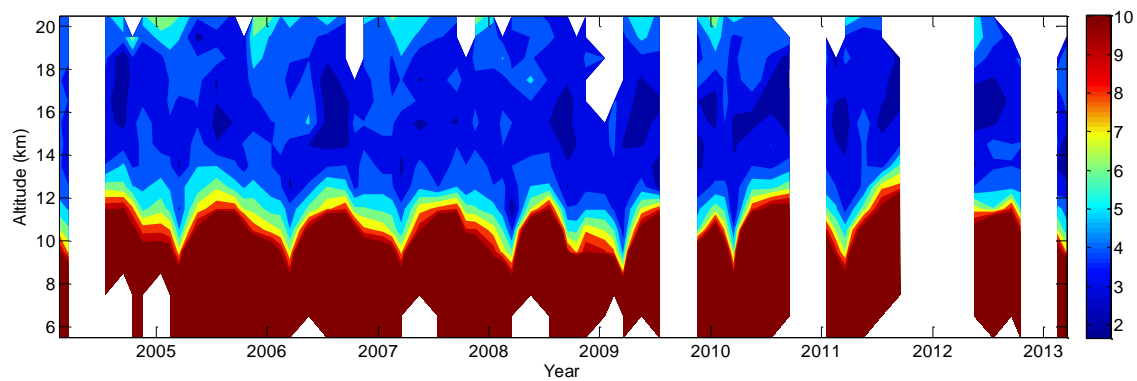
8

9

10

11

12



1

2 Figure 3. Time series of the MAESTRO monthly median water vapour volume mixing ratio
3 (VMR) versus altitude (km) at northern high latitudes (60-90°N). The time series is composed
4 using the eight months in which ACE samples the northern high latitudes (see Sect. 2).

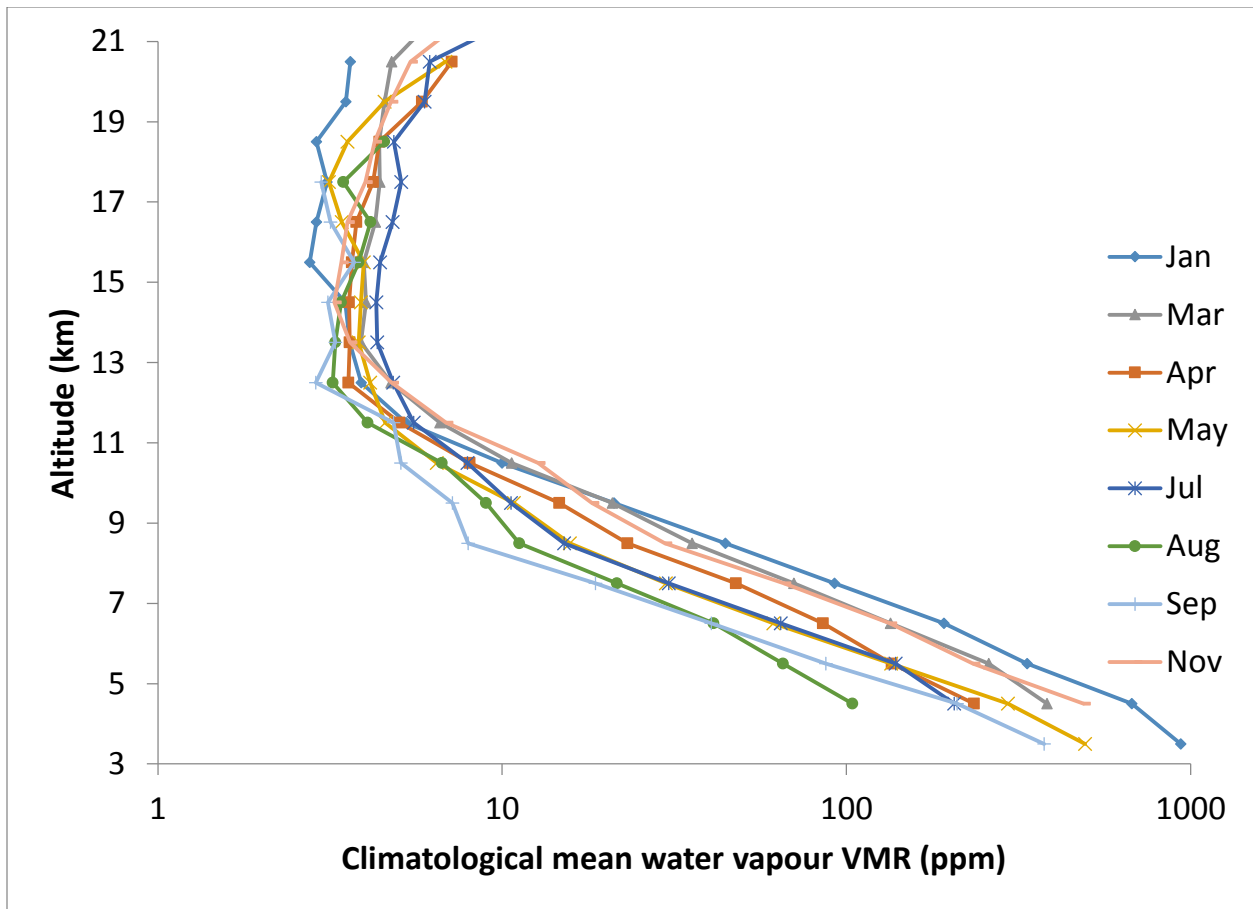
5

6

7

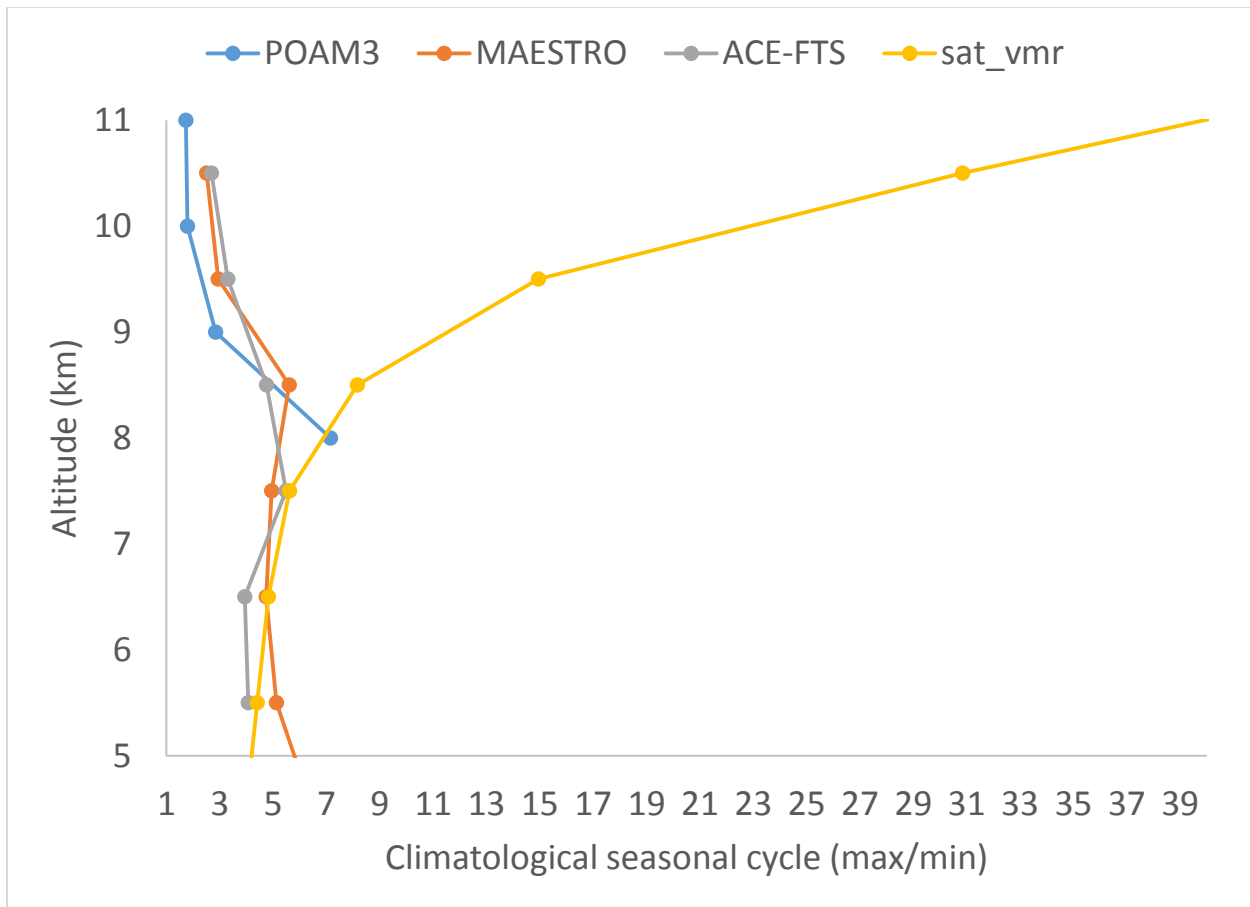
8

9

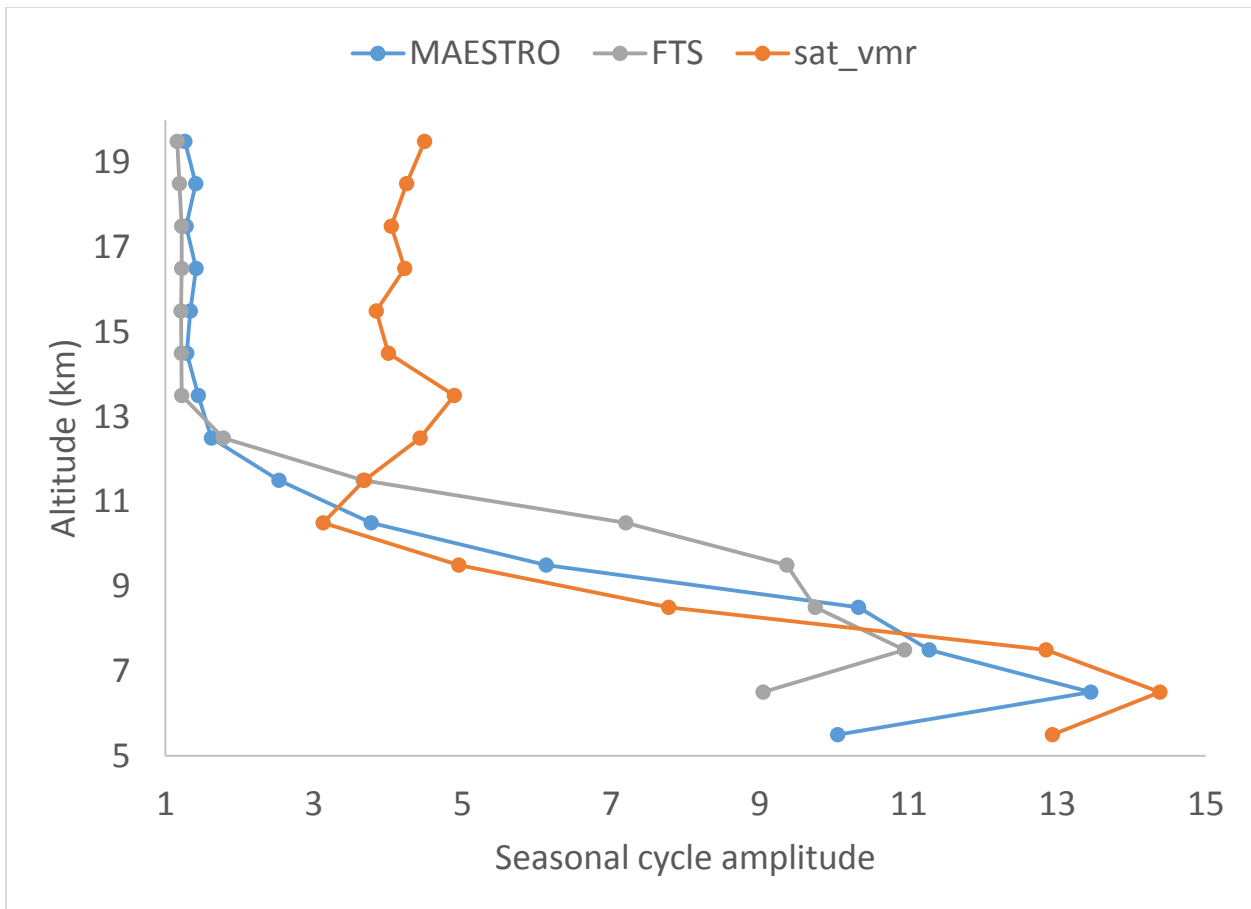


1

2 Figure 4. MAESTRO mean climatology (2004-2012) of the vertical distribution of water vapour
 3 volume mixing ratio in the Antarctic (60-90°S) UT/LS for months with sufficient sampling of
 4 the region. A logarithmic scale is used for the x-axis.

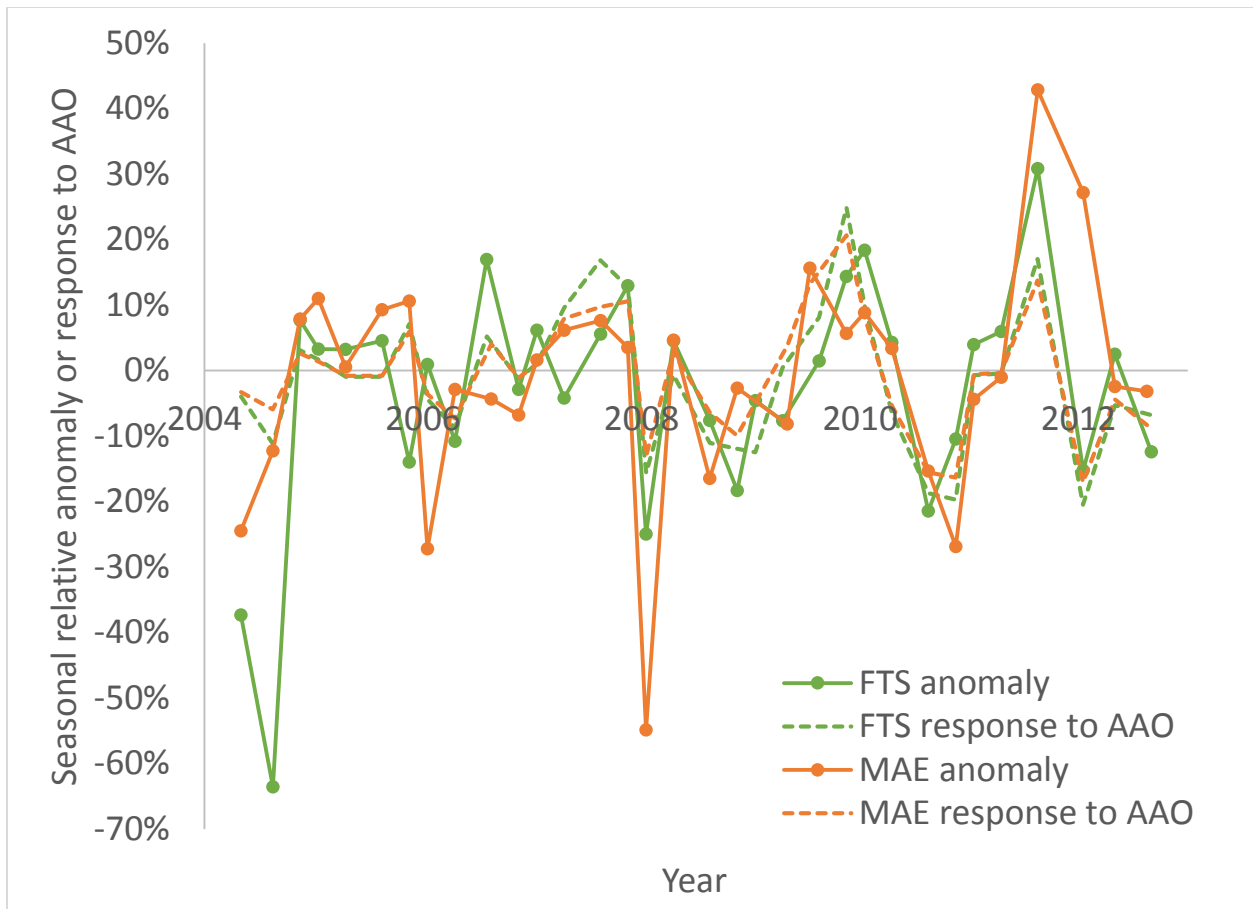


1
 2 Figure 5. Vertical profile of the seasonal cycle amplitude of Antarctic water vapour observed by
 3 three instruments. The amplitude is calculated by taking the ratio of climatological monthly
 4 means at maximum (January or December) and minimum (August or September). Note that
 5 POAM III has a different orbit that tends to sample consistently at higher latitudes (Nedoluha et
 6 al., 2002) and thus tends to have stronger seasonality at 8 km (driven by the larger temperature
 7 range). The saturation vapour pressure climatology is obtained using GEM analysis
 8 temperatures sampled at ACE measurement locations.

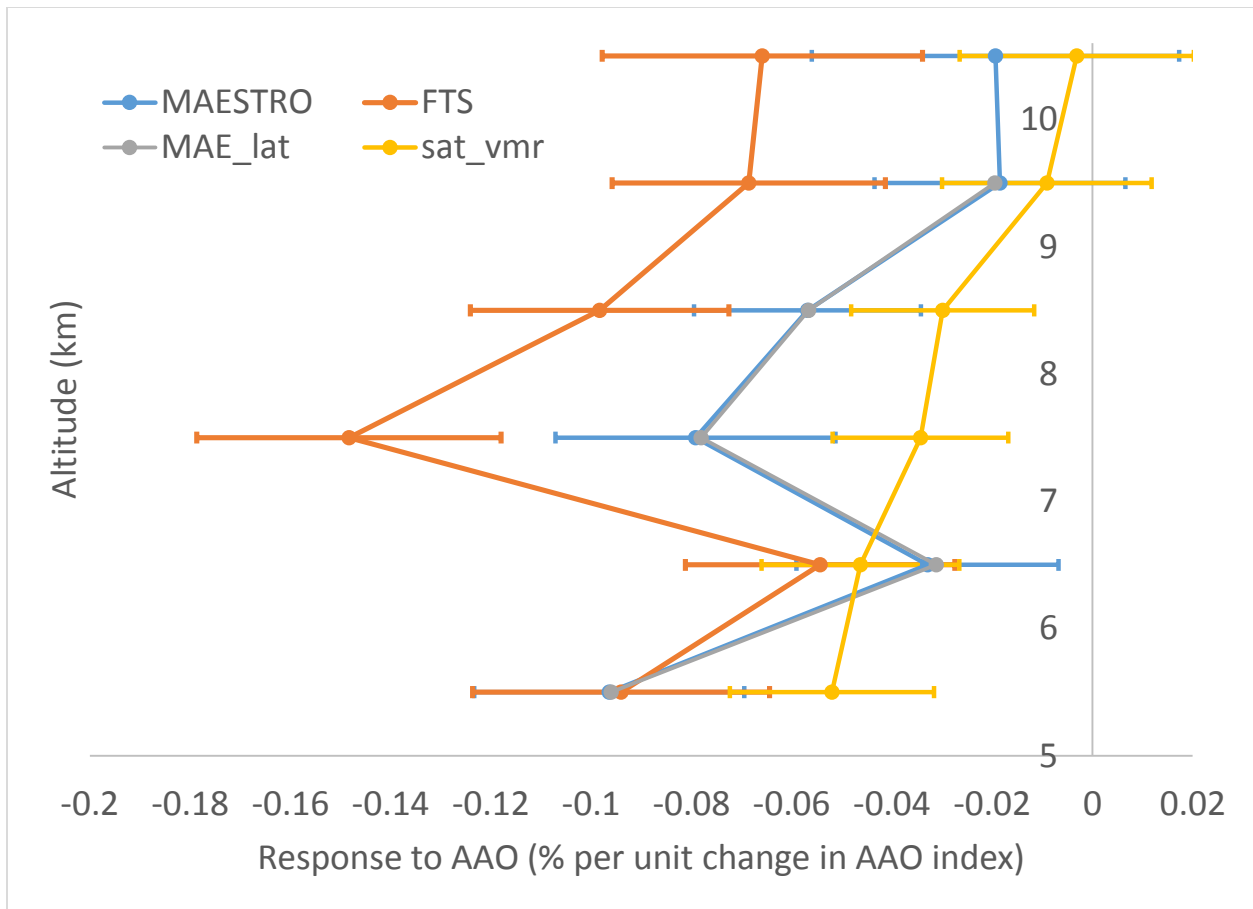


1

2 Figure 6. Analogous to Fig. 5 but for northern high latitudes. Profiles are presented at their
 3 respective native vertical resolutions.

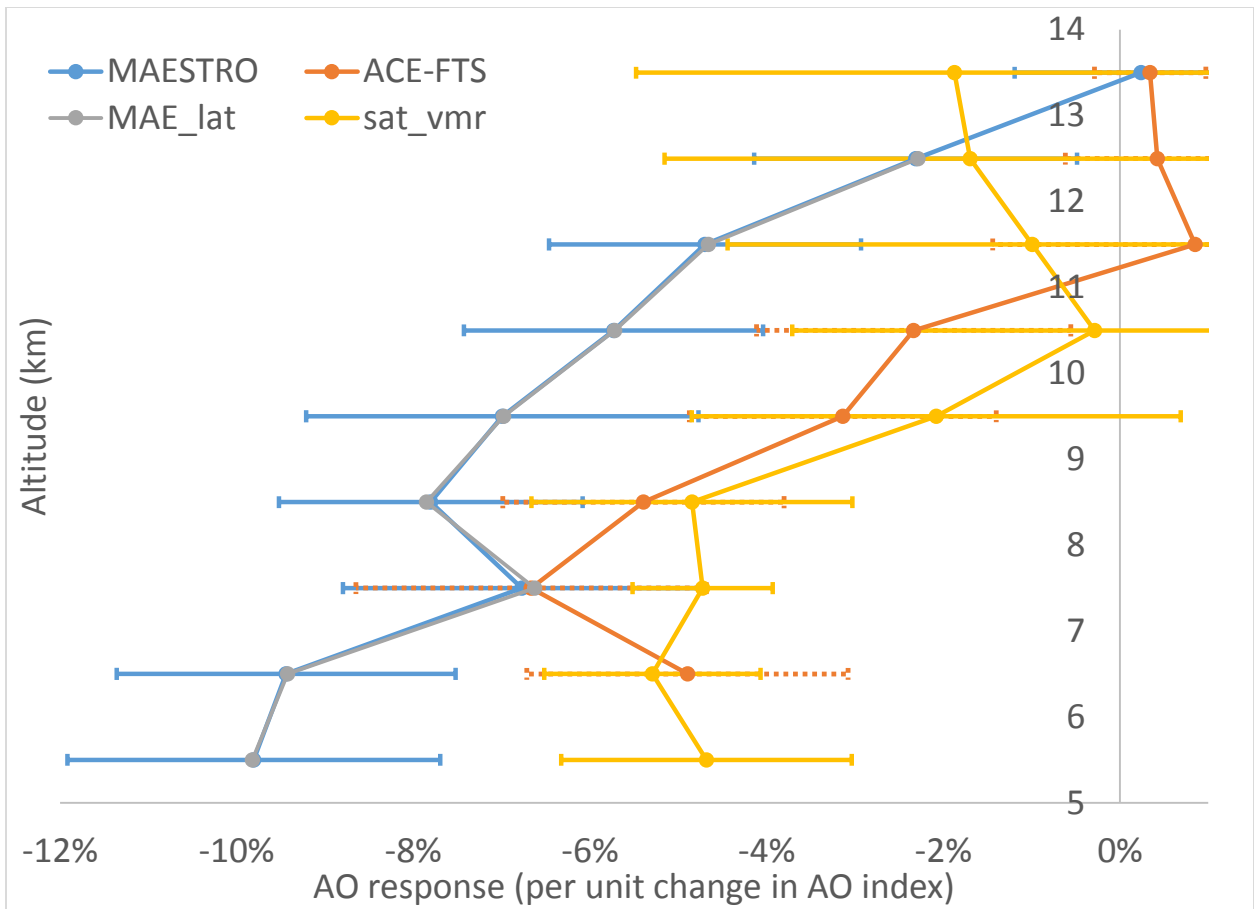


1
 2 Figure 7. Seasonal median water vapour anomaly time series from MAESTRO (8.5 km) and
 3 ACE-FTS (7.5 km) in the Antarctic troposphere and the response of each to AAO determined by
 4 linear regression. Seasons with missing data are removed to avoid discontinuities. The markers
 5 on the response curves indicate the sampled seasons.



1
 2 Figure 8. Vertical profile of response to AAO, using southern high latitude water vapour relative
 3 anomalies based on monthly medians (2004-2012). Horizontal bars are $\pm 1\sigma$, obtained by linear
 4 regression (including a trend term and/or a Puyehue proxy term depending on whether each is
 5 significant at the 1σ level). The “MAE_lat” profile shows the MAESTRO water vapour response
 6 to AAO upon including a basis function to account for the non-uniform latitudinal sampling. The
 7 ‘sat_vmr’ profile is obtained from a simple linear regression of saturation VMR relative
 8 anomalies onto AAO.

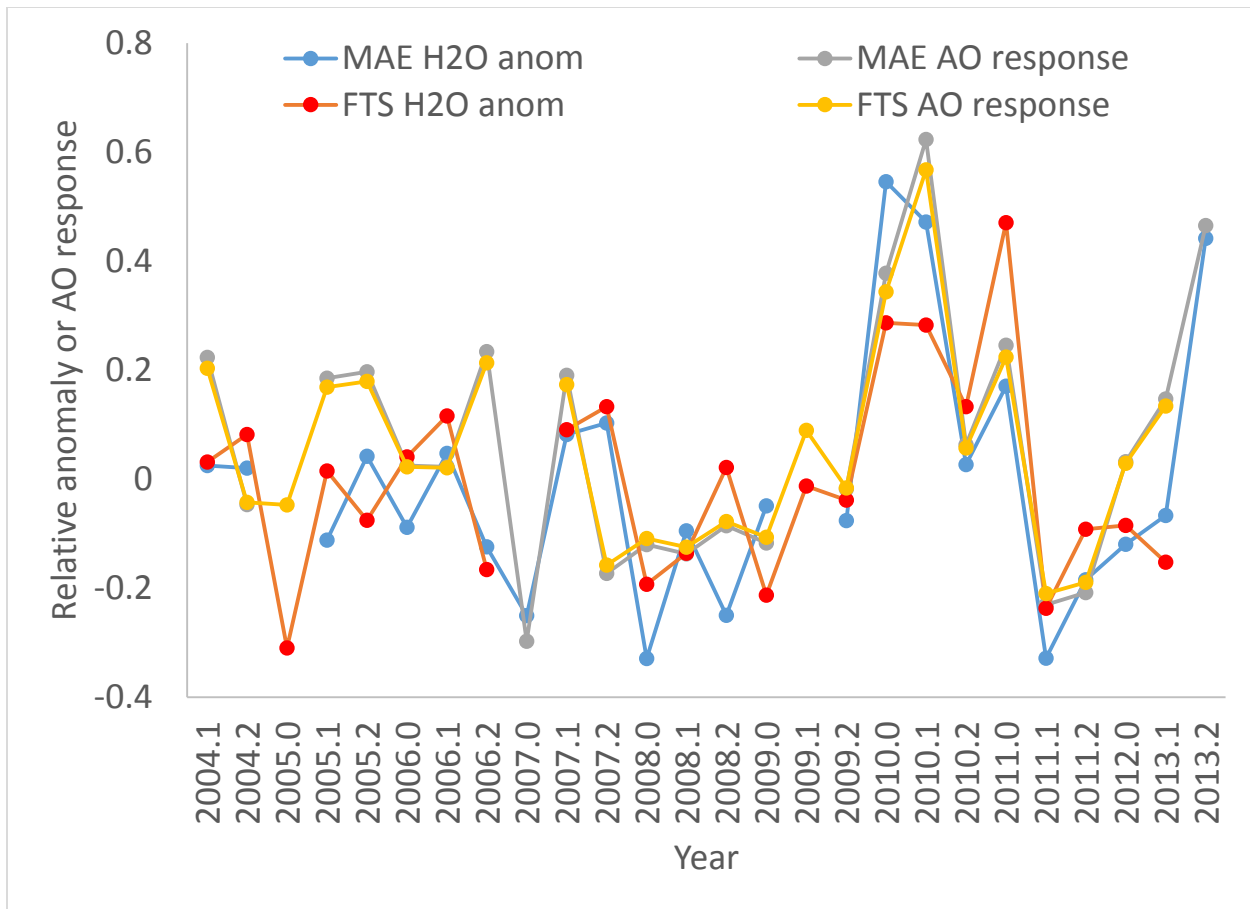
9



1

2 Figure 9. Analogous to Fig. 8, but for northern high latitudes water vapour in response to the
 3 Arctic oscillation. Error bars display ± 1 standard error of the fitting coefficient for the AO index
 4 obtained by linear regression. At 5.5 km, the response of ACE-FTS is not shown since it has a
 5 standard error of $>100\%$ and the sample size decreases significantly.

6



1
 2 Figure 10. Time series of water vapour relative anomalies observed by ACE-MAESTRO
 3 (“MAE”) and ACE-FTS at 6.5±0.5 km in winter months (January-March). Slight differences in
 4 sampling exist between the two instruments due to the requirement for >20 observations per
 5 month per altitude bin.